PNAS RESEARCH ARTICLE | ECOLOGY
ENVIRONMENTAL SCIENCES

Widespread use of proton-pumping rhodopsin in Antarctic phytoplankton

Sarah M. Andrew[a], Carly M. Moreno[a,1], Kaylie Plumb[b], Babak Hassanzadeh[c], Laura Gomez-Consarnau[c,d], Stephanie N. Smith[a], Oscar Schofield[e], Susumu Yoshizawa[f], Takayoshi Fujiwara[f], William G. Sunda[a], Brian M. Hopkinson[b], Alecia N. Septer[a], and Adrian Marchetti[a,2]

Edited by Edward DeLong, University of Hawai'i at Manoa, Honolulu, HI; received May 6, 2023; accepted August 13, 2023

Photosynthetic carbon (C) fixation by phytoplankton in the Southern Ocean (SO) plays a critical role in regulating air–sea exchange of carbon dioxide and thus global climate. In the SO, photosynthesis (PS) is often constrained by low iron, low temperatures, and low but highly variable light intensities. Recently, proton-pumping rhodopsins (PPRs) were identified in marine phytoplankton, providing an alternate iron-free, light-driven source of cellular energy. These proteins pump protons across cellular membranes through light absorption by the chromophore retinal, and the resulting pH energy gradient can then be used for active membrane transport or for synthesis of adenosine triphosphate. Here, we show that PPR is pervasive in Antarctic phytoplankton, especially in iron-limited regions. In a model SO diatom, we found that it was localized to the vacuolar membrane, making the vacuole a putative alternative phototrophic organelle for light-driven production of cellular energy. Unlike photosynthetic C fixation, which decreases substantially at colder temperatures, the proton transport activity of PPR was unaffected by decreasing temperature. Cellular PPR levels in cultured SO diatoms increased with decreasing iron concentrations and energy production from PPR photochemistry could substantially augment that of PS, especially under high light intensities, where PS is often photoinhibited. PPR gene expression and high retinal concentrations in phytoplankton in SO waters support its widespread use in polar environments. PPRs are an important adaptation of SO phytoplankton to growth and survival in their cold, iron-limited, and variable light environment.

proton-pumping rhodopsin | high-light | iron | Southern Ocean | retinal

Rhodopsins are ubiquitous retinal-based light-adsorbing proteins that can perform a variety of light-mediated cellular functions. Proton-pumping rhodopsins (PPRs) were initially described in halophilic archaea over half a century ago (1) and subsequently identified in marine heterotrophic bacteria (2), yet were only recently discovered in marine heterotrophic and autotrophic protists (3–6). However, their specific cellular location and function have remained elusive. In bacterial PPRs, light adsorption isomerizes all-trans retinal to 13-cis retinal, driving a series of reactions that pump a proton across the membrane in which the protein is embedded. Because PPRs in bacteria colocalize with ATP (adenosine triphosphate) synthases and transporters in the same membrane surrounding the cell, the resulting proton gradient can then be used for membrane active transport, ATP synthesis and other cellular functions (2, 7). Expression of proteorhodopsins (PRs) in bacterioplankton is common across different marine environments (8, 9), including Antarctic coastal waters (10). Based on current evidence, bacterial PPRs may absorb as much light energy as photosynthetic light-harvesting complexes (11), yet it is unclear whether the membrane pH gradients generated by PPR light absorption are used primarily for ATP synthesis, as opposed to other physiological functions such as active membrane transport (7, 12, 13).

Recently, PPRs were discovered in marine diatoms and other phytoplankton; however, their subcellular localization and biological function are unclear. Its presence in marine phytoplankton from iron-limited regions, such as the SO, suggests a role in alleviating iron stress (3, 14, 15). Unlike the iron-rich protein components of the photosynthetic apparatus, PPRs are simple proteins and do not contain iron and thus should be less adversely impacted by low SO iron levels. While it is generally accepted that photosynthesis (PS) is the primary mechanism for cellular energy production in phytoplankton, it now seems plausible that PPR-containing phytoplankton could use PPRs to augment light-driven proton transport across cellular membranes to supplement cellular energy production by PS and provide an alternative source of ATP (16).

Phytoplankton carbon (C)-fixation in the polar SO plays an important role in the global transfer of C from the atmosphere to the ocean's interior, accounting for 40% of anthropogenic C uptake (17, 18), but this C-fixation is often limited by low iron availability,

Significance

Proton-pumping rhodopsins (PPRs) are retinal-binding membrane proteins that function as light-driven proton pumps to create proton gradients across cell membranes, which can be used for active membrane transport and production of cellular energy. We show that PPR in Southern Ocean (SO) diatoms is localized to the vacuole, making it an alternative phototrophic organelle. Estimates of energy flux through PPR in SO diatoms suggest that PPR could produce significant amounts of cellular energy under low temperature, low iron, and high light conditions. Use of PPR was found to be widespread in the SO and increases in low iron regions. These findings point to PPRs being an important adaptation of SO phytoplankton for their growth and survival, impacting the global carbon cycle.

Author contributions: S.M.A., B.M.H., A.N.S., and A.M. designed research; S.M.A., C.M.M., K.P., B.H., L.G.-C., S.N.S., O.S., S.Y., T.F., B.M.H., A.N.S., and A.M. performed research; S.M.A., C.M.M., W.G.S., B.M.H., A.N.S., and A.M. analyzed data; and S.M.A., W.G.S., and A.M. wrote the paper.

The authors declare no competing interest.

This article is a PNAS Direct Submission.

[1]Present Address: Marine Microbial Ecology Laboratory, Biology Program, New York University Abu Dhabi, Abu Dhabi 129188, United Arab Emirates.

[2]To whom correspondence may be addressed. Email: amarchetti@unc.edu.

This article contains supporting information online at https://www.pnas.org/lookup/suppl/doi:10.1073/pnas.2307638120/-/DCSupplemental.

Published September 18, 2023.

cold temperatures and low light levels (19). In addition, SO phytoplankton are often exposed to highly variable light conditions caused by deep mixing in near-surface ocean waters (20). In response to these harsh growth conditions, SO phytoplankton have distinct biochemical adaptations to overcome slow enzymatic reaction rates at cold temperatures and the high iron costs associated with PS (21). The active use of PPR by SO phytoplankton may represent an important part of these adaptations. In this study, we sought to understand the ecological role of PPR in Antarctic phytoplankton by integrating data derived from experiments across broad biological scales, including in vitro protein analysis, physiological characterization and energy budgets, and community-level expression in situ, to present a model for how PPR could support the survival of SO phytoplankton and promote oceanic C uptake.

Results and Discussion

Characterization of PPRs in Polar Diatoms. Eukaryotic protist PPRs can be split into distinct clades, where diatom PPRs are closest to the xanthorhodopsin (XR) clade found in Gloeobacter bacteria that contain a second carotenoid chromophore, salinixanthin (3, 22). Recently, additional rhodopsin-carotenoid complexes have been characterized in diverse XR and PR-containing aquatic microorganisms (23). PPRs have been identified in some, but not all, phytoplankton, with variability at the species level, suggesting acquisition through horizontal gene transfer events from bacteria followed by subsequent gene losses. Alignment of diatom PPRs from the temperate diatom *Pseudo-nitzschia granii* and a closely related SO diatom *Pseudo-nitzschia subcurvata* supports the idea

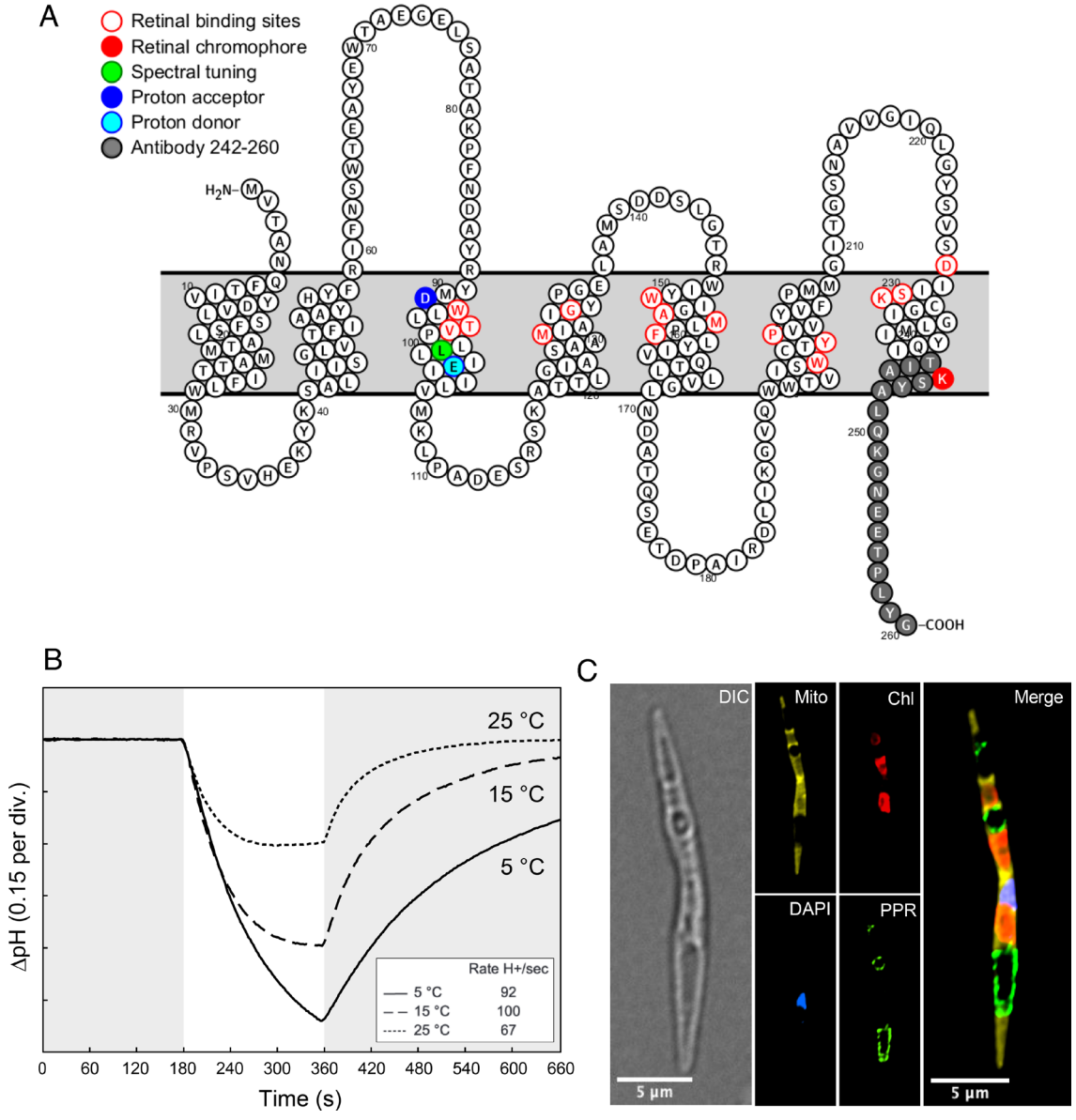

Fig. 1. Characterization of PPR in the polar diatom *P. subcurvata*. (*A*) Predicted secondary structure of the *P. subcurvata* PPR (29). Single-letter amino acid codes are used, and numbers correspond to positions. Functional residues are highlighted as follows: retinal binding pockets (red borders), retinal chromophore covalent attachment (K, red), proton acceptor (D; blue), spectral tuning (L; green), proton donor (E, cyan), and epitope for antibody (dark gray). (*B*) Light-induced outward proton pump activity (measured as pH changes) at 5, 15, and 25 °C for suspensions of *E. coli* cells containing the expression plasmid for *P. subcurvata* PPR. The white-filled region indicates the period of illumination. (*C*) Cellular localization of *P. subcurvata* PPR performed using immunofluorescence assay with an antibody raised against the C-terminal peptide. Images are differential interference contrast (DIC) light micrograph, MitoTracker staining (Mito) for mitochondria, red fluorescence for chloroplasts (Chl), DAPI for DNA, *P. subcurvata* PPR antibody (PPR), and a merge of all four. White bars = 5 µm. Brightness and contrast adjustments were made uniformly across images from all treatments using FIJI. See Movie S1 for a 360° video rendering.

that these are proton pumping rhodopsins, where functional sites and spectral tuning residues are conserved across species and align well with functionally annotated SAR86 PR (8) (*SI Appendix*, Fig. S1). The leucine residue (position 105 in SAR86 PR) suggests that retinal, the light-harvesting pigment in PPRs, is tuned to green light absorption (24); Fig. 1*A*). Further characterization of diatom PPR from *P. granii* confirms maximum absorbance of light at 511 nm (green light) and demonstrates functional proton pumping abilities when expressed in *Escherichia coli*, similar to that of bacterial PRs (22). Both the sequence homology and heterologous expression of diatom PPR in *E. coli* suggest that they pump from the cytoplasm across the plasma membrane of bacterial cells. Initial proton-pumping rates by diatom PPR in the *E. coli* expression system were independent of temperature (Fig. 1*B*); but over time, larger pH differences were observed at colder temperatures, presumably due to decreased proton diffusion rates back across cellular membranes (25). By contrast photosynthetic rates slow substantially with decreasing temperature (26, 27, 28). Thus, proton pumping rates of PPR should increase relative to photosynthetic rates with decreasing temperature, with important implications for the frigid waters of the SO.

To better understand the potential biological function for phytoplankton PPR, it was important to identify where this protein was localized within the cell. Immunofluorescence provides an unbiased approach for visualizing intracellular protein localization via fluorescence microscopy. An antibody was developed against the C-terminal residues of the *P. subcurvata* PPR protein (Fig. 1*A*), and the specificity of the resulting antibody was confirmed against total protein extracts by western blotting, resulting in a single, abundant protein band of the predicted size (~29 kDa) (*SI Appendix*, Fig. S2). PPR occurred in multiple, distinct ring-like structures in iron-limited *P. subcurvata* cells that did not colocalize with the organelles forming the nucleus (DAPI), mitochondria (Mito), or chloroplasts (Fig. 1*C*, *SI Appendix*, Fig. S3, and Movie S1), suggesting that PPR is likely bound to the vacuolar membrane. Diatom vacuoles are acidic (30), and PPR in the vacuolar membrane would promote vacuolar acidity through light-driven proton-pumping into the vacuole. The clear visualization of PPR in iron-limited *P. subcurvata* indicates that this mechanism is active under low iron conditions and informs our model of energetic proton flux within the cell under these conditions.

A PPR-generated proton gradient across the vacuolar membrane could serve to supplement cellular energy in several ways. ATP synthases produce ATP from the pH gradient across photosynthetic and mitochondrial membranes (31), but they also may occur in vacuolar membranes, providing an additional source of ATP in PPR-containing phytoplankton. Moreover, although the Vacuolar-ATPases (V-ATPases) are thought to use ATP to pump protons into the vacuole, PPR activity could supplement proton pumping by V-ATPases, thereby conserving photosynthetically produced ATP, which is restricted under low-iron conditions (Fig. 2). In addition, light-driven PPR acidification of the vacuole could allow the vacuolar V-ATPases to function in reverse, thereby generating ATP (4), although it is unclear whether diatom V-ATPases are bidirectional as observed in vitro for other eukaryotic cells (32). Other plausible functional roles include diatom PPR working in conjunction with vacuolar-type H^+ pyrophosphatase to create pyrophosphate, which can supplement ATP as an energy currency in phototrophs (33). A proton gradient across the vacuolar membrane could also mediate the active transport of

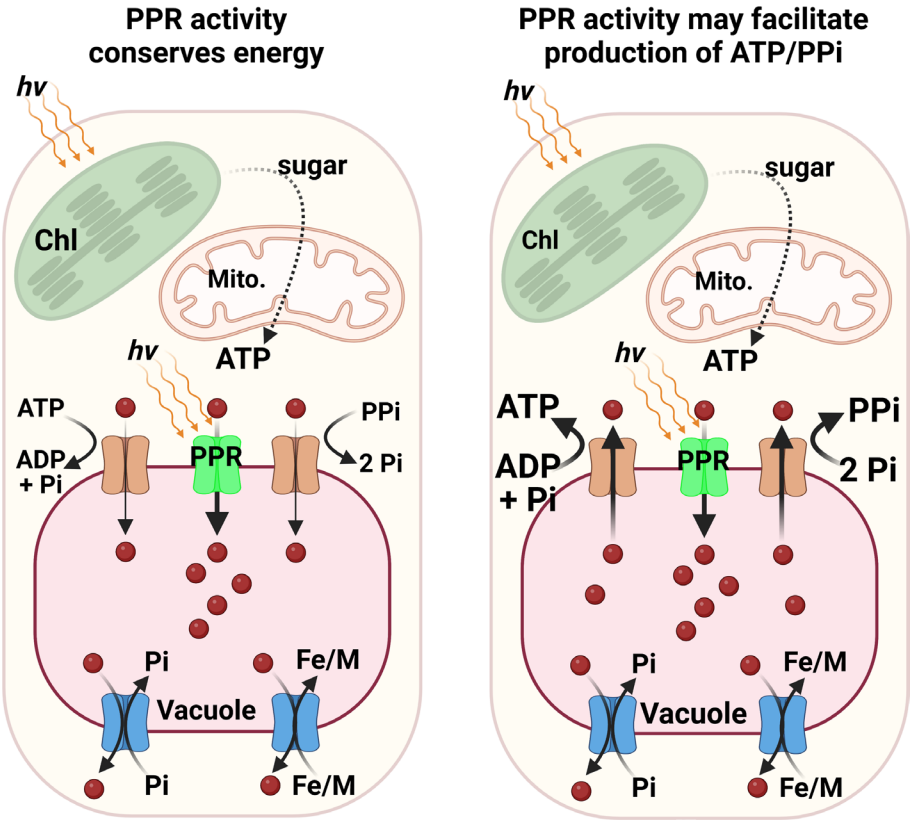

Fig. 2. Diatom cell schematics showing light-driven proton (H^+) transport into the vacuole by PPR under low iron conditions, which is supplemented by vacuolar H^+ transport by VATPase and V-PPase enzymes under low light (or high iron) conditions. The resulting membrane pH gradient fuels active transport of inorganic phosphate (Pi), iron (Fe) and other metals (M), and other biologically needed molecules into the vacuole. The PPR-generated membrane pH gradient could also be used to run VTPase and V-PPase enzymes in reverse, thereby generating cellular ATP (*Right*), although direct evidence for this is currently lacking. Created with BioRender.com.

nutrients (e.g., iron and phosphate) and other biological molecules across the vacuolar membrane by driving transporters and inorganic ion exchangers (7). Finally, other previous experimental data suggest that diatom PPR may also be localized in the plastid outer membrane, possibly serving to acidify the intermembrane space to facilitate C fixation (22). Together, these findings underscore the importance of localizing PPR in diverse phytoplankton species, as the subcellular location of PPR dictates its biological function.

Diatom PPR Contributions to Cellular Energy. PS is heavily dependent on iron due to the large amounts required in various protein components (PSII [2-3 Fe], Cyt b_6/f [5 Fe], PSI [12 Fe], ferredoxin [2 Fe]), constituting a majority of the cellular iron (21, 34). By contrast, PPR contains no iron, thus its function should be unaffected by iron-limiting conditions (3, 16). To better understand how PPR may contribute to cellular energetics relative to PS, we estimated the potential energy flux for PS and PPR in SO diatoms. Laboratory experiments were conducted in cultures of three recently isolated PPR-containing SO diatoms to determine the effect of iron limitation on specific growth rate and cellular PPR concentrations. We used retinal levels as a proxy for PPR concentration because retinal can be easily quantified and is incorporated into PPR at a one-to-one ratio (35, 36). In experiments run at a growth-saturating light intensity (100 mmol photons m^{-2} s^{-1}), a decrease in total iron concentration from 1,370 nmol L^{-1} to 1.5 or 3.1 nmol L^{-1} decreased maximum PSII photosynthetic efficiencies and specific growth rates by 20 to 38% in *P. subcurvata* and *Chaetoceros socialis* but had no significant effect in *Synedra hyperbola* (Fig. 3 *A* and *B*). The decrease in iron concentration increased retinal:cellular C ratios by 32 to 100% in all three species (Fig. 3*C*), and surprisingly, the largest effect occurred in *S. hyperbola*, where retinal:C ratios were highest, consistent with previous findings of increased PPR gene expression and protein concentrations under low-iron growth conditions (3).

Diatom PPR energy flux rates in the culture experiments were estimated from cellular retinal:C ratios, light intensity, and PPR photophysiological characteristics. In contrast to the conventional photosynthetic system, which is composed of multiple protein complexes linked by electron shuttles, PPR is a single membrane-embedded protein with one retinal chromophore whose photoactivation leads to cross-membrane proton transit. This simple architecture facilitates estimation of its energy production from first principles (*Methods*). At the low growth-saturating light intensity of our experimental cultures, diatom PPR was well below its saturation irradiance (~2,000 µmol photons m^{-2} s^{-1}), contributing from <1% to ~7% of total cellular energy production, with the percent energy flux by PPR generally higher under low-iron growth conditions (Fig. 3*D*). However, because PS is typically at its maximum in SO phytoplankton at our experimental light intensity (100 µmol photons m^{-2} s^{-1}) and

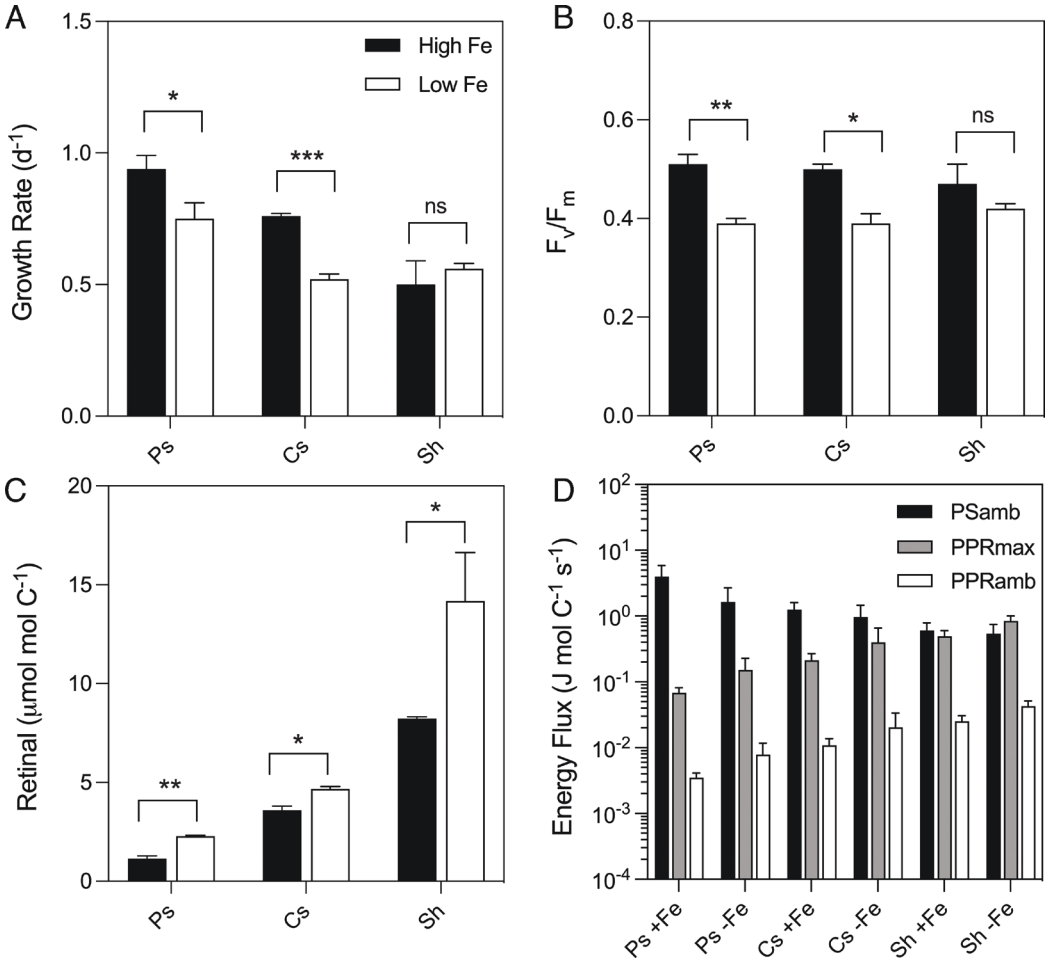

Fig. 3. Proton-pumping rhodopsin energy contributions in polar diatoms under iron-replete and iron-limiting growth conditions. (*A*) Specific growth rates (d^{-1}); (*B*) PSII maximum photochemical efficiency (Fv/Fm); (*C*) cellular retinal concentrations normalized to carbon, and (*D*) estimated energy fluxes from PS and PPR under saturating (PPRmax) and ambient irradiance levels (PSamb and PPRamb) in the polar diatoms *P. subcurvata* (Ps), *Chaetoceros sociales* (Cs), and *Synedra hyperborea* (Sh) under high-iron (+Fe) and low-iron (−Fe) conditions. Asterisks indicate *P* values where * is <0.05, ** is <0.001, *** is <0.0001, and ns is not significant. Error bars denote the SD of replicates (n ≥ 3).

is subject to photoinhibition in SO phytoplankton at modest light intensities at or above 400 µmol photons m^{-2} s^{-1} (28, 37), the contribution of PPR to total cellular energy flux would increase substantially at the higher light levels found in shallow SO mixed layers during summer or in microalgae living in the arctic sea ice in late spring or early summer. At the maximum solar light intensity found at the surface of the SO [e.g., 1,500 µmol photons m^{-2} s^{-1} at Palmer Research Station on the Antarctic Peninsula (38)], energy flux by PPR photochemistry would be much higher than that at our experimental light intensity while PS would likely be lower owing to photoinhibition (28, 37). Furthermore, photoinhibition is particularly severe in iron-limited phytoplankton owing to the increased production of reactive oxygen species under iron limitation of PS, and the presence of iron in important antioxidant enzymes (iron superoxide dismutase, ascorbate peroxidase, and catalase), which remove toxic superoxide radicals and hydrogen peroxide, thereby preventing the formation of highly toxic hydroxyl radicals (39, 40). Thus, PPR may be critical to the growth and survival of phytoplankton in high-light, near-surface environments in the iron-limited SO and in allowing cells to survive highly variable light conditions associated with deep wind-driven surface mixed layers commonly occurring in many regions of the SO (20).

PPR Distribution in the Southern Ocean (SO). To examine PPR distribution associated with protists in SO marine habitats, retinal concentrations in larger cells (>5 µm) and rhodopsin gene expression (*RHO*), which includes genes encoding for PPRs, were examined along the Palmer Long-Term Ecological Research (Pal-LTER) transect located to the west of the West Antarctic Peninsula (WAP) (*SI Appendix*, Fig. S4). These waters encompass steep environmental gradients with relatively warmer, ice-free stations to the north and colder stations to the south, adjacent to the seasonal sea ice edge. Onshore to offshore waters constitute east to west transects, where western-most offshore stations frequently contain the lowest iron concentrations resulting in iron-limited phytoplankton communities (41). Taxonomic annotation of *RHO* from RNA sequencing of near-surface phytoplankton showed that the majority of transcripts belonged to photosynthetic dinoflagellates, diatoms, and haptophytes (*SI Appendix*, Fig. S5). Across all stations, *RHO* transcripts associated with dinoflagellates were most highly expressed, but also occurred in the haptophyte Phaeocystis and pennate diatoms such as Fragilariopsis and Pseudo-nitzschia, a genus of SO diatom used here for PPR localization and energetic estimates (Figs. 1 and 3).

Concentrations of the PPR chromophore retinal measured by liquid chromatography–mass spectrometry (LC–MS) were highest at coastal stations associated with high levels of chlorophyll *a* (Chl *a*) from a bloom of the diatom *Actinocyclus* (Fig. 4*A*). Retinal concentrations within the bay were some of the highest ever recorded [e.g., 112 and 342 pM; (11, 15)]. The highest retinal values normalized to phytoplankton Chl *a* were measured at the offshore stations, particularly in the central region of the Pal-LTER sampling grid, suggesting a higher abundance of PPR in phytoplankton at these locations.

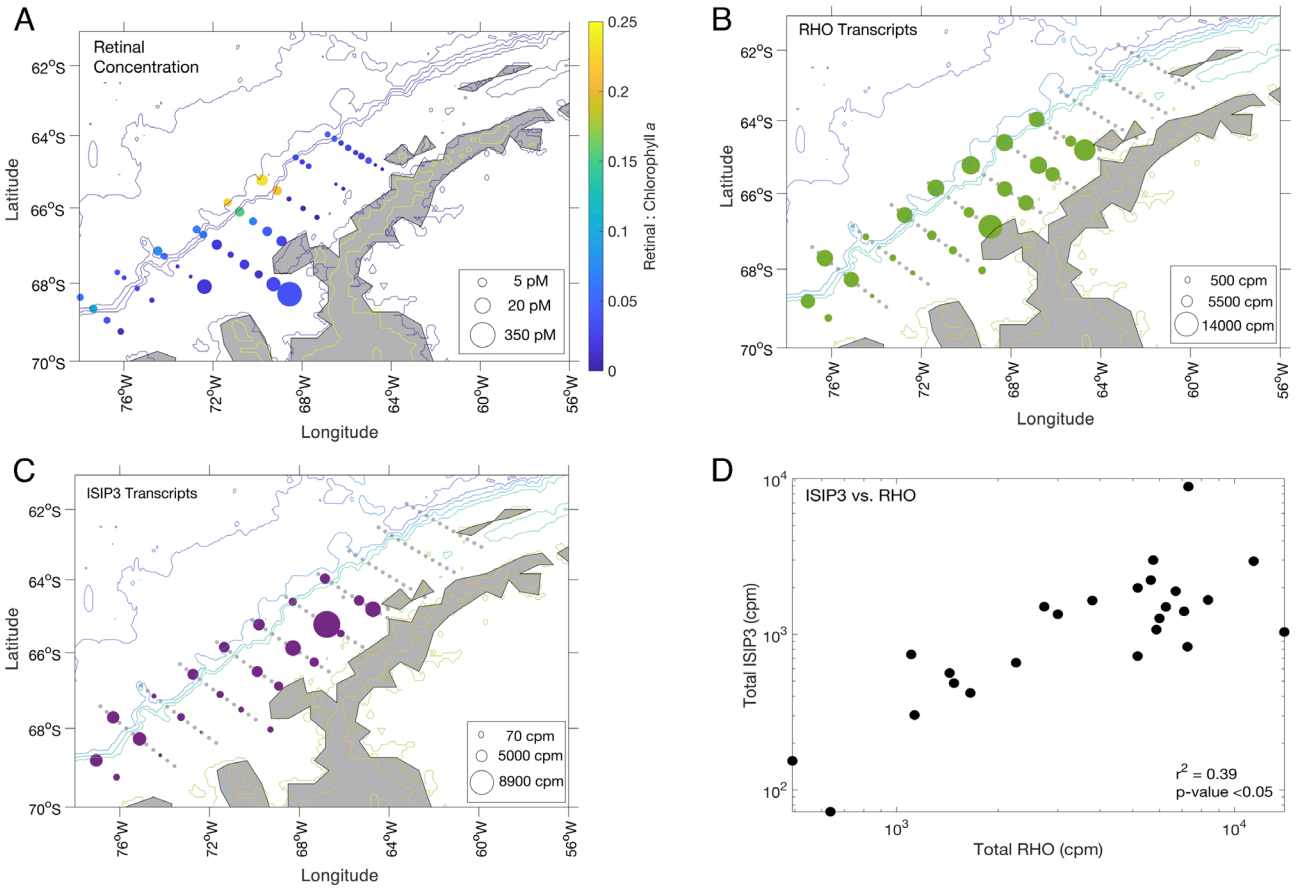

Fig. 4. Eukaryotic rhodopsin in the West Antarctic Peninsula along the Pal-LTER sampling grid. (*A*) Absolute (circle size) and relative concentrations (circle color) of retinal (the chromophore in PPR) at select stations. Relative retinal concentrations are normalized to chl *a* concentrations. (*B*) Diatom-associated rhodopsin (*RHO*) gene expression and (*C*) iron-starvation-induced protein 3 (*ISIP3*) gene expression at select stations. Summed target gene transcripts for annotated diatom genera are individually normalized to total transcripts for each diatom to generate counts per million reads (cpm). (*D*) Correlation analysis of diatom *ISIP3* transcripts vs. *RHO* gene transcripts. Pearson correlation coefficient (r) and *P* value are indicated.

The relative abundance of diatom-associated *RHO* transcripts throughout the Pal-LTER grid was also highest in the central regions of the grid, with all offshore stations containing high *RHO* gene expression compared to the southern, onshore stations (Fig. 4*B*). *RHO* gene expression correlated with transcript abundance of the Iron-Starvation-Induced Protein 3 (*ISIP3*) in diatoms ($r = 0.39$, $P < 0.05$) (Fig. 4 *C* and *D*), whose expression increases in iron-limited diatoms and is used as a molecular indicator of low iron stress (42, 43). Thus, trends in retinal:Chl *a* and gene expression across the Pal-LTER grid suggest that higher cellular PPR levels are associated with low-iron stressed phytoplankton, consistent with the results of our culture studies.

Implications for SO Phytoplankton. There are specific instances where cellular energy potentially supplied from PPR may be favored over that from oxygenic PS (16). As noted earlier, at a typical SO temperature of −1.8 to 4 °C, PS becomes light-saturated at light intensities at or below 60 to 80 μmol photons m^{-2} s^{-1}

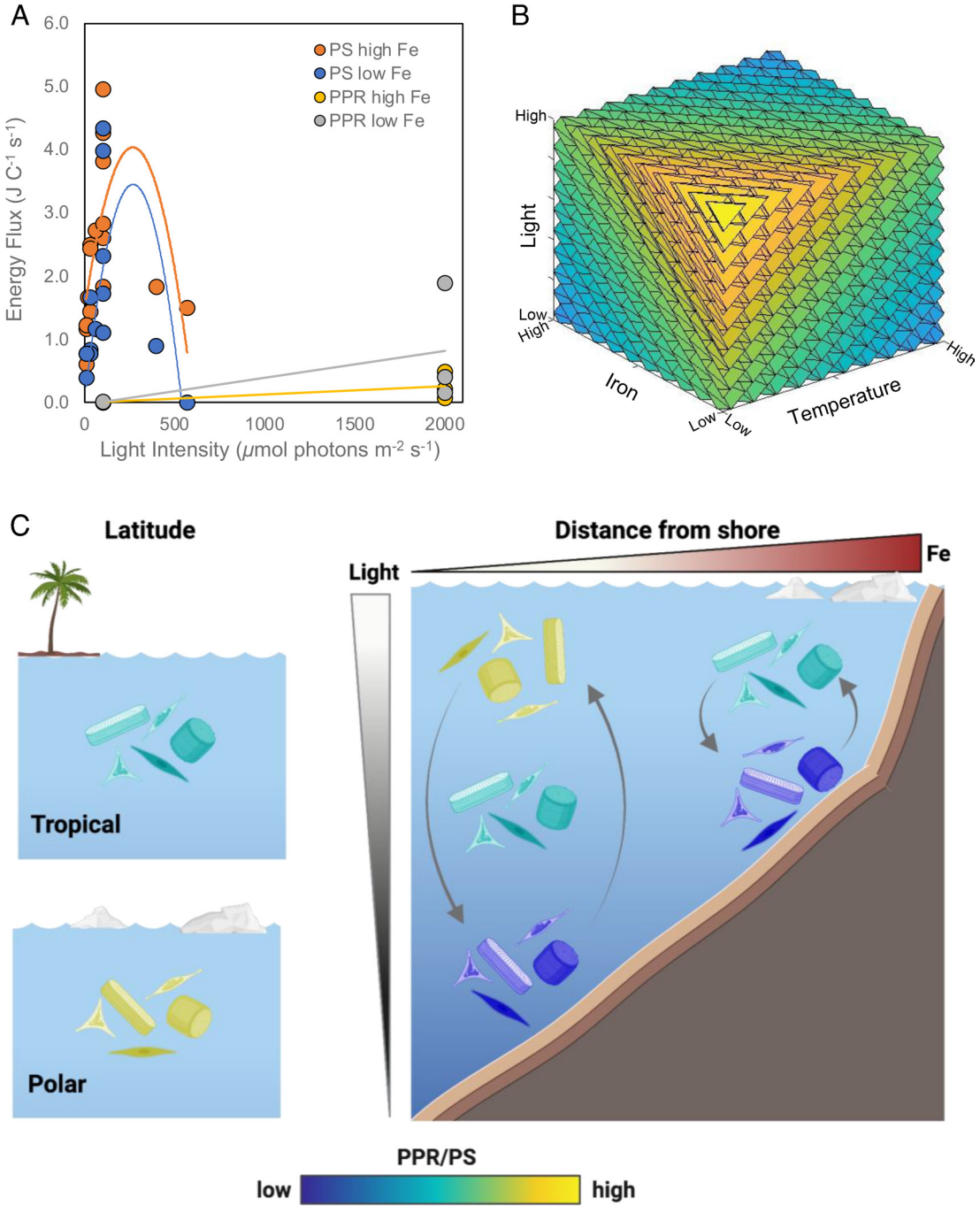

Fig. 5. Environmental conditions favoring the use of PPRs in phytoplankton. (*A*) Estimates of cellular energy flux as a function of light intensity in high-iron and low-iron polar phytoplankton. Photosynthetic energy fluxes were estimated from growth rates as a function of light intensity and iron growth conditions as measured in this study and Strzepek et al. (28) (*Methods*). Estimates from high-iron and low-iron cultures are plotted along with the average trendlines. (*B*) Estimated energy production from PPR to PS ratio as a function of iron concentration, temperature, and light intensity. (*C*) Conceptual diagram of ocean regions distinguished by latitude and distance from shore along with conditions throughout the euphotic zone where PPR would be favored over PS. Light = light intensity and Fe = iron concentration. Color scale of PPR/PS ratios applies to (*B*) and (*C*) and is in relative units. Fig. 5*C* was created with BioRender.com.

(4 to 5% of maximum surface noon light intensity on a cloudless day; ~1,500 μmol photons m^{-2} s^{-1}) (28) and is photoinhibited at light intensities above ~500 μmol photons m^{-2} s^{-1}, an effect that is enhanced under iron limitation (26). By contrast, PPR proton pumping rates become light saturated at a much higher light intensity (~2,000 μmol photons m^{-2} s^{-1}) and should not experience photoinhibition (Fig. 5*A*). Thus, PPR reaction rates are not only favored relative to PS at the colder temperatures of the SO but also at the higher light intensities and low iron concentrations of near-surface waters (Fig. 5*B*). A similar model has recently been proposed for a PPR-containing bacterium within alpine lakes, where reliance on XR-based ATP synthesis is favored over anoxygenic PS under high-light, low-temperature conditions (44). In marine phytoplankton, this may be important with respect to biological energy production in deep wind-driven surface mixed layers of the SO, where cells may be continually mixed from deeper depths where there is insufficient light for PS, into intermediated depths where PS is favored, and then into surface waters where energy production by PPR photochemistry may dominate cellular energy supply (Fig. 5*C*).

Thus, the presence of PPR may be critical to the growth and survival of phytoplankton in the SO. Our findings support this notion, and the widespread use of PPR within Antarctic phytoplankton likely represents an evolutionary adaptation to the extreme SO conditions of low iron, low temperature, and highly variable light conditions, providing them with an additional source of cellular energy production within this turbulent, energy-deprived environment. These findings have important implications for biological C fixation in the SO, and subsequent transport to the ocean's interior in the SO, an important process regulating atmospheric CO_2 and global climate.

Materials and Methods

Polar Diatom Isolates and Sequencing. The polar diatoms *P. subcurvata* (UNC1901), *Chaetoceros cf. sociales* (UNC1905), and *Synedra hyperborea* (UNC1904) were isolated from the Western Antarctic Peninsula along the Pal-LTER sampling grid in 2019. Isolates were identified by morphological characteristics and 18S rRNA gene sequencing (*SI Appendix*, Table S1). As *Pseudo-nitzschia* species are often difficult to identify by their 18S rRNA gene sequence, additional confirmation of the taxonomic identification of *P. subcurvata* was provided through sequencing of the 18S-ITS1-5.8S region as described in Hubbard, Rocap, and Armbrust (45). Transcriptomes were also sequenced (14), leading to the identification of PPR gene sequences in each of the isolates (*SI Appendix*, Table S1).

Antibody Design and Immunofluorescence Microscopy. A synthetic peptide with the sequence TIAKSYALQKGNEETPLYG, matching the C terminus of the *P. subcurvata* PPR (Fig. 1*A*) was produced by Pacific Immunology and used to immunize two rabbits. Monoclonal antibodies were affinity-purified, and the final product was tested for specificity against crude protein extracts from multiple diatom cultures by western blotting.

For immunofluorescence microscopy, cells were collected by filtration and incubated in 100 nM MitoTracker Red (Invitrogen) for 30 min in the dark and then fixed with 4% glutaraldehyde in 1× PBS buffer containing 67 mM EGTA (pH 7.5). After 30 min, cells were washed five times in 0.1% Triton X-100 in PBS buffer over 15 min. Subsequently, cells were rinsed with Tris Buffered Saline (TBS) and blocked with 0.5% bovine serum albumin (BSA) in TBS buffer for 60 min. Cells were rinsed an additional five times before incubation with the primary antibody diluted 1:500 in TBS overnight at 4 °C, rinsed five times with TBS + blocking reagent, and then incubated with Goat Anti-Rabbit IgG (H/L):FITC (BioRad, 5196-2404) diluted 1:500 in TBS overnight at 4 °C. Cells were finally rinsed with TBS, incubated with DAPI, and then mounted in a 35-mm glass-bottomed dish. Images were captured using an inverted Nikon Ti2 fluorescence microscope outfitted with a Hamamatsu ORCA Fusion sCMOS camera. Images were processed using Nikon NIS-Elements software. Brightness and contrast adjustments were made uniformly for all images in a given experiment.

Proton Transport Activity. Light-driven proton transport activity of PPR was measured from light-induced pH changes of suspensions of *E. coli* cells expressing *P. granii* PPR. The full-length cDNA for *P. granii* rhodopsin (accession no. AJA37445.1), whose codons were optimized for *E. coli*, was chemically synthesized by Eurofins Genomics and inserted into the NdeI-XhoI site of the pET21a(+) vector as described in ref. 22. Protein expressions were then induced at 37 °C for 3 to 4 h by adding 0.1 mM isopropyl β-D-1-thiogalactopyranoside and 10 μM all-trans retinal (Sigma- Aldrich, St. Louis, MO, USA). The rhodopsin-expressing cells were collected by centrifugation (4,400 × g for 3 min), washed three times in 100 mM NaCl, and resuspended in 6 mL 100 mM NaCl for measurements. Light-induced pH changes were monitored using a Horiba F-72 pH meter. All measurements were conducted at 5, 15 and 25 °C using a thermostated reaction cell (Eyela NCB-1200, Tokyo Rikakikai Co. Ltd, Japan). The initial rate of proton transport was estimated from the slope of measured pH vs. time for the first 30 s of light exposure.

Diatom Growth Rates and Photophysiology. Polar diatom isolates were maintained at 4 °C under constant irradiance at a light intensity of 100 μmol photons m^{-2} s^{-1} within media containing high (1,370 nmol L^{-1}) and low (1.5 nmol L^{-1}, 3.1 nmol L^{-1} for *S. hyperborea*) iron concentrations. Cultures were grown in 1 L polycarbonate bottles in the synthetic seawater medium AQUIL, enriched with filter sterilized vitamins and a trace metal buffer containing 100 μM ethylenediaminetetraacetic acid (EDTA) (46). Growth media also contained 300 μM nitrate, 200 μM silicic acid, and 20 μM phosphate. Fe bound to EDTA was added for a total iron concentration of either 1,370 or 1.5 nM (3.1 nM for *S. hyperborea*) to achieve iron-replete and iron-limited growth rates, respectively. All cells were preacclimated to each treatment's iron concentration for at least three transfers before reported growth rates, and other measurements were collected. All media were prepared and cultures subsampled in a positive-pressure, trace metal clean laminar flow hood. Specific growth rates of successive transfers were calculated from linear regression of the natural log of in vivo chl a fluorescence using a Turner Designs model 10-AU (47). Photophysiological characteristics of PSII were measured with a Fluorescence Induction Relaxation System (Satlantic) set to measure single-turnover flash of PSII reaction centers with a total of 50 iterations (48). Triplicate subsamples were low-light adapted at ~10 μmol photons m^{-2} s^{-1} for at least 30 min. A saturating pulse of blue light (450 nm) was applied to low-light acclimated cells for a duration of 80 ms using the reference excitation profile. Maximum photochemical efficiency of PSII (F_v/F_m) was determined using the induction and relaxation protocol.

Gross Oxygen Production. As a measure of cellular energy generation from conventional PS, gross dioxygen (O_2) production rates were measured via membrane inlet mass spectrometry. Rates of gross oxygen production and respiration in the light were measured using $^{18}O_2$ and a membrane inlet mass spectrometer (MIMS) (49). Cultures were concentrated by gentle filtration (<5 in. Hg), resuspended in media, and placed in an MIMS chamber. Most of the ambient O_2 was removed by bubbling with N_2 gas, and a bubble of $^{18}O_2$ was added by syringe and allowed to exchange with the solution until the total O_2 reached concentrations originally present in the culture. PS was induced by shining a light into the sample of the same intensity at which they were grown (100 μmol photons m^{-2} s^{-1}). Gross oxygen production and respiration in the light were determined from measured rates of $^{16}O_2$ production and $^{18}O_2$ consumption. These rates were converted to energy production using a 1:1 ratio of O_2 production to C fixation and canonical energy requirements for CO_2 fixation (479 kJ mol^{-1}; Johnson 2016). The bulk of cellular energy generated by the photosynthetic light reactions is used to fix CO_2 making this a reasonable estimate of total energy generation from the photosynthetic system.

PPR Energy Generation. The contribution of PPR to the total energy budget was estimated to determine if it could play an important role in metabolic energy generation. PPR's simple architecture facilitates estimation of its energy production from first principles as

$$E_{PR} = \Delta G_{H+}[PPR] * T * S_{H+},$$

where ΔG_{H+} is the transmembrane proton energy gradient (estimated as 18 kJ mol^{-1}), PPR is the rhodopsin concentration in mol $cell^{-1}$, t is the turnover rate of PPR per second, and S_{H+} is the proton stoichiometry (protons pumped per turnover; assumed to be 1) (50). We estimated the PPR energy generation

rate under two light intensities, the experimental growth-saturating photosynthetically active radiation (PAR) intensity (100 mmol photons m^{-2} s^{-1}) and the maximum sea-surface solar PAR intensity for the SO measured at the Palmer Research Station, Antarctica (1,500 μmol photons m^{-2} s^{-1}). The maximum retinal H^+ pumping rate (equal to its maximum turnover rate of 300 ms^{-1} (22) occurs at a light intensity of ~2,000 μmol photons m^{-2} s^{-1}, above the maximum solar light intensity in the SO. The PPR turnover rate (t) was computed from the equation:

$$\tau = \Phi \sum_i \sigma_i E_i ,$$

where Φ is the quantum yield for reaction [estimated as 0.5; (51)], i is an index over all relevant wavelengths, s_i is the optical absorption cross-section at wavelength i, and E_i is the culture irradiance at wavelength i. PPR per cell was determined from retinal concentrations, which were measured using the methods described below. Retinal is the chromophore in PPR and is not known to have any other major biochemical roles in phytoplankton and so its abundance serves as a proxy for cellular PPR concentrations.

Retinal Quantification. Retinal concentrations in the diatom isolates and field samples were determined by liquid-chromatography tandem mass spectrometry (LC–MS/MS) according to refs. (11, 15). The LC–MS/MS apparatus consisted of a Thermo Accela™ LC system (refrigerated autosampler and LC pump) coupled to a Thermo TSQ™ Quantum Access™ heated electrospray ionization triple quadrupole mass spectrometer. Further detailed methods for retinal quantification are provided in supplemental information. Retinal-to-C ratios of the diatom isolates were estimated by dividing cellular retinal concentrations by cellular C concentrations, as determined using a Costech 4010 CHNOS elemental combustion system.

Pal-LTER Sampling. The Pal-LTER study region is located along the western coast of the Antarctic Peninsula, encompassing an area of approximately 140,000 km^2 (*SI Appendix*, Fig. S4). The sampling grid is 700 km north to south, with major grid lines spaced 100 km apart running from onshore to offshore, perpendicular to the peninsula. The individual stations are spaced 20 km along each grid line (52). The grid is frequently divided into subregions based on latitude and hydrographic and sea ice conditions (53). The North consists of lines 600 to 400, the South consists of lines 300 and 200, and the Far South consists of lines 100 to −100. Moving from onshore to offshore, stations 0.000 to 0.040 are within the coastal region, station 0.100 is within the shelf region, and stations 0.190 and 0.200 are over the continental slope. The sampling for this study occurred during the Pal-LTER 2018 austral summer research cruise (30 December 2017 to 12 February 2018) aboard the R/V Laurence M. Gould.

Chl *a* concentrations were obtained as part of the Pal-LTER core measurements. Briefly, seawater samples were collected from Niskin bottles deployed throughout the water column (with casts typically including 0 m, or at least one observation between 0 and 5 m) or from the ship's surface seawater flow-through system. Filters for Chl *a* analysis were frozen and stored at −80 °C and then measured by fluorescence (54). For retinal concentrations, approximately 1.5 to 4 L of surface seawater was collected (depending on biomass) and filtered through a 5-μm pore-size polycarbonate filter (47 mm, Millipore) and immediately stored at −80 °C. Samples were kept frozen on dry ice during shipment to the US. Retinal was extracted, and concentrations were determined as described above.

For RNA analysis, approximately 2 to 4 L of surface seawater was collected (depending on biomass) and filtered through a 47-mm, 0.2-μm-pore Supor filter (Millipore). Each filter was preserved in 1 mL of RNA later and stored at −80 °C. Samples were kept frozen on dry ice during shipment to the United States. Total RNA was extracted with the RNAqeuous 4PCR Kit (Ambion) according to the manufacturer's instructions with the addition of an initial 1-min bead beating step using acid-washed sterile glass beads (Sigma Aldrich) to ensure that cells were disrupted and mechanically removed from the filter. Samples were individually barcoded and pooled prior to sequencing on a single lane of the Illumina HiSeq 4000 platform. Sequencing resulted in *ca.* 15 million 2 × 150 bp paired-end reads per sample. Sequences were quality filtered with Trimmomatic v0.38 and assembled as described in ref. 55. A consensus assembly was representative of all expressed genes of the microeukaryote community along the WAP and was used in the subsequent annotation and read count steps. For functional annotations, consensus sequences were searched against the Kyoto Encyclopedia of Genes and Genomes (KEGG) database v2018 by similarly using Diamond BLASTX and a 10^{-5} e-value. Because KEGG only provides KOs for functionally annotated genes, KEGG gene definitions for iron-starvation-induced proteins (*ISIP*s) and *RHO* sequences were manually performed (55). Taxonomic annotations of *RHO* and *ISIP3* were assigned using Diamond BLASTX v2.0.4 based on homology (e-value cutoff of 10^{-5}) to PhyloDB v1.075, a custom database curated by the Allen Lab (Scripps Oceanographic Institute), consisting of eukaryotic genomes and the transcriptomes from the Marine Microbial Eukaryote Transcriptome Sequencing Project. We further supplemented the database with eight polar transcriptomes isolated from the WAP and previously sequenced (14), which included the transcriptomes of *P. subcurvata* and *C.* cf. *sociales*, as well as *S. hyperborea* that was sequenced as part of this study.

Sequence Data Deposition. The 18S rRNA gene and *RHO* sequences for polar diatoms *P. subcurvata* (UNC1901), *Chaetoceros cf. sociales* (UNC1905), and *S. hyperborea* (UNC1904) are deposited in National Center for Biotechnology Information Genbank (*SI Appendix*, Table S1). Raw reads for the Pal-LTER metatranscriptome sequencing are deposited in SRA BioProject accession no. PRJNA877830 (56).

Data, Materials, and Software Availability. Raw reads for the Pal-LTER metatranscriptome sequencing; 18S rRNA and RHO genes data have been deposited in SRA BioProject; GenBank (PRJNA877830 (56); *SI Appendix*, Table S1).

ACKNOWLEDGMENTS. We thank M. Meyer, E. Speciale, and P. Lim for assistance with figure construction and sequence submissions and O. Torano for assistance with energy flux experiments. We are grateful to the captain and crew of the ARSV Lawrence M. Gould as well as the participants of the Pal-LTER 2018 cruise for assistance with collection of the WAP data. Portions of the paper were developed from the thesis of C.M.M. This work was funded by the NSF Grants OPP1745036 (to A.N.S. and A.M.), OPP1744760 (to B.M.H.), and PLR1440435 (to O.S.).

Author affiliations: [a]Department of Earth, Marine, and Environmental Sciences, University of North Carolina at Chapel Hill, Chapel Hill, NC 27599; [b]Department of Marine Sciences, University of Georgia, Athens, GA 30602; [c]Department of Biological Sciences, University of Southern California, Log Angeles, CA 90089; [d]Departamento de Oceanografía Biológica, Centro de Investigación Científca y de Educación Superior de Ensenada, Ensenada, Baja California 22860, Mexico; [e]Department of Marine and Coastal Sciences, Rutgers University, New Brunswick, NJ 08901; and [f]Atmosphere and Ocean Research Institute, The University of Tokyo, Chiba 277-8564, Japan

1. D. Oesterhelt, W. Stoeckenius, Rhodopsin-like protein from the purple membrane of Halobacterium halobium. *Nat. New Biol.* **233**, 149–152 (1971).
2. O. Béjà *et al.*, Bacterial rhodopsin: Evidence for a new type of phototrophy in the sea. *Science* **289**, 1902–1906 (2000).
3. A. Marchetti, D. Catlett, B. M. Hopkinson, K. Ellis, N. Cassar, Marine diatom proteorhodopsins and their potential role in coping with low iron availability. *ISME J.* **9**, 2745–2748 (2015).
4. C. H. Slamovits, N. Okamoto, L. Burri, E. R. James, P. J. Keeling, A bacterial proteorhodopsin proton pump in marine eukaryotes. *Nat. Commun.* **2**, 183 (2011).
5. A. Marchetti *et al.*, Comparative metatranscriptomics identifies molecular bases for the physiological responses of phytoplankton to varying iron availability. *Proc. Natl. Acad. Sci. U.S.A.* **109**, E317–E325 (2012).
6. T. Mock *et al.*, Evolutionary genomics of the cold-adapted diatom Fragilariopsis cylindrus. *Nature* **541**, 536–540 (2017).
7. J. A. Fuhrman, M. S. Schwalbach, U. Stingl, Proteorhodopsins: An array of physiological roles? *Nat. Rev. Microbiol.* **6**, 488–494 (2008).
8. J. R. d. l. Torre, *et al.*, Proteorhodopsin genes are distributed among divergent marine bacterial taxa. *Proc. Natl. Acad. Sci. U.S.A.* **100**, 12830–12835 (2003).
9. O. Béjà, E. N. Spudich, J. L. Spudich, M. Leclerc, E. F. DeLong, Proteorhodopsin phototrophy in the ocean. *Nature* **411**, 786–789 (2001).
10. J. Cifuentes-Anticevic *et al.*, Proteorhodopsin phototrophy in antarctic coastal waters. *mSphere* **6**, e0052521 (2021).
11. L. Gómez-Consarnau *et al.*, Microbial rhodopsins are major contributors to the solar energy captured in the sea. *Sci. Adv.* **5**, eaaw8855 (2019).
12. J. M. Walter, D. Greenfield, C. Bustamante, J. Liphardt, Light-powering *Escherichia coli* with proteorhodopsin. *Proc. Natl. Acad. Sci. U.S.A.* **104**, 2408–2412 (2007).
13. E. F. DeLong, O. Béjà, The light-driven proton pump proteorhodopsin enhances bacterial survival during tough times. *PLoS Biol.* **8**, e1000359 (2010).
14. C. M. Moreno *et al.*, Examination of gene repertoires and physiological responses to iron and light limitation in Southern Ocean diatoms. *Polar Biol.* **41**, 679–696 (2018).
15. B. Hassanzadeh *et al.*, Microbial rhodopsins are increasingly favoured over chlorophyll in high nutrient low chlorophyll waters. *Environ. Microbiol. Rep.* **13**, 401–406 (2021).
16. J. A. Raven, Functional evolution of photochemical energy transformations in oxygen-producing organisms. *Funct. Plant Biol.* **36**, 505–515 (2009).

17. C. L. Sabine *et al.*, The oceanic sink for anthropogenic CO2. *Science* **305**, 367–371 (2004).
18. M. C. Long *et al.*, Strong Southern Ocean carbon uptake evident in airborne observations. *Science* **374**, 1275–1280 (2021).
19. P. W. Boyd, Environmental factors controlling phytoplankton processes in trhe Southern Ocean. *J. Phycol.* **38**, 844–861 (2002).
20. B. G. Mitchell, E. A. Brody, O. Holm-Hansen, C. McClain, J. Bishop, Light limitation of phytoplankton biomass and macronutrient utilization in the Southern Ocean. *Limnol. Oceanogr.* **36**, 1662–1677 (1991).
21. R. F. Strzepek, P. W. Boyd, W. G. Sunda, Photosynthetic adaptation to low iron, light, and temperature in Southern Ocean phytoplankton. *Proc. Natl. Acad. Sci. U.S.A.* **116**, 4388–4393 (2019).
22. S. Yoshizawa *et al.*, Light-driven proton pumps as a potential regulator for carbon fixation in marine diatoms. *Microb. Environ.* **38**, ME23015 (2023).
23. A. Chazan *et al.*, Phototrophy by antenna-containing rhodopsin pumps in aquatic environments. *Nature* **615**, 535–540 (2023).
24. D. Man *et al.*, Diversification and spectral tuning in marine proteorhodopsins. *EMBO J.* **22**, 1725–1731 (2003).
25. K. Y. Cheong *et al.*, Saturation of thylakoid-associated fatty acids facilitates bioenergetic coupling in a marine diatom allowing for thermal acclimation. *Glob. Change Biol.* **27**, 3133–3144 (2021).
26. A. Neori, O. Holm-Hansen, Effect of temperature on rate of photosynthesis in Antarctic phytoplankton. *Polar Biol.* **1**, 33–38 (1982).
27. R. W. Eppley, Temperature and phytoplankton growth in the sea. *Fish. Bull.* **70**, 1063–1085 (1972).
28. R. F. Strzepek, K. A. Hunter, R. D. Frew, P. J. Harrison, P. W. Boyd, Iron-light interactions in Southern Ocean phytoplankton. *Limnol. Oceanogr.* **57**, 1182–1200 (2012).
29. U. Omasits, C. H. Ahrens, S. Müller, B. Wollscheid, Protter: Interactive protein feature visualization and integration with experimental proteomic data. *Bioinformatics* **30**, 884–886 (2014).
30. J. Raven, The role of vacuoles. *New Phytolog.* **106**, 357–422 (1987).
31. P. G. Falkowski, J. A. Raven, *Aquatic Photosynthesis (Second Edition)* (Princeton University Press, ed. STU–Student edition, 2007).
32. D. J. Cipriano *et al.*, Structure and regulation of the vacuolar ATPases. *Biochim. Biophys. Acta* **1777**, 599–604 (2008).
33. M. Maeshima, Vacuolar H+-pyrophosphatase. *Biochim. Biophys. Acta Biomembr.* **1465**, 37–51 (2000).
34. J. A. Raven, The iron and molybdenum use efficiencies of plant growth with different energy, carbon and nitrogen sources. *New Phytolog.* **1988**, 279–287 (1988).
35. D. Bownds, Site of attachment of retinal in rhodopsin. *Nature* **216**, 1178–1181 (1967).
36. K. Palczewski *et al.*, Crystal structure of rhodopsin: A G protein-coupled receptor. *Science* **289**, 739–745 (2000).
37. S. Trimborn, S. Thoms, K. Bischof, S. Beszteri, Susceptibility of two southern ocean phytoplankton key species to iron limitation and high light. *Front. Mar. Sci.* **6**, 167 (2019).
38. J. Sherman, M. Y. Gorbunov, O. Schofield, P. G. Falkowski, Photosynthetic energy conversion efficiency in the West Antarctic Peninsula. *Limnol. Oceanogr.* **65**, 2912–2925 (2020).
39. W. G. Sunda, S. A. Huntsman, Effect of Zn, Mn, and Fe on Cd accumulation in phytoplankton: Implications for oceanic Cd cycling. *Limnol. Oceanogr.* **45**, 1501–1516 (2000).
40. K. K. Niyogi, Photoprotection revisited: Genetic and molecular approaches. *Annu. Rev. Plant Physiol. Plant Mol. Biol.* **50**, 333–359 (1999).
41. A. L. Annett *et al.*, Controls on dissolved and particulate iron distributions in surface waters of the Western Antarctic Peninsula shelf. *Mar. Chem.* **196**, 81–97 (2017).
42. P. D. Chappell *et al.*, Genetic indicators of iron limitation in wild populations of *Thalassiosira oceanica* from the northeast Pacific Ocean. *ISME J.* **9**, 592–602 (2015).
43. C. M. Moreno, W. Gong, N. R. Cohen, K. DeLong, A. Marchetti, Interactive effects of iron and light limitation on the molecular physiology of the Southern Ocean diatom Fragilariopsis kerguelensis. *Limnol. Oceanogr.* **65**, 1511–1531 (2020).
44. K. Kopejtka *et al.*, A bacterium from a mountain lake harvests light using both proton-pumping xanthorhodopsins and bacteriochlorophyll-based photosystems. *Proc. Natl. Acad. Sci. U.S.A.* **119**, e2211018119 (2022).
45. K. A. Hubbard, G. Rocap, E. V. Armbrust, Inter- and intra-specific community structure within the diatom genus *Pseudo-nitzschia* (Bacillariophyceae). *J. Phycol.* **44**, 637–649 (2008).
46. N. M. Price *et al.*, Preparation and chemistry of the artificial algal culture medium Aquil. *Biol. Oceanogr.* **6**, 443–461 (1989).
47. L. E. Brand, W. Sunda, R. R. L. Guillard, A method for the rapid and precise determination of acclimated phytoplankton reproductive rates. *J. Plankton Res.* **3**, 193–201 (1981).
48. M. Y. Gorbunov, P. Falkowski, "Fluorescence Induction and Relaxation (FIRe) technique and instrumentation for monitoring photosynthetic processes and primary production in aquatic ecosystems" in *Proceedings of 13th International Congress of Photosynthesis*, A. van der Est, D. Bruce, Eds. (Allen Press, Montreal, 2005), pp. 1029–1031.
49. T. M. Kana, Relationship between photosynthetic oxygen cycling and carbon assimilation in *Synechococcus* WH7803 (cyanophyta). *J. Phycol.* **28**, 304–308 (1992).
50. W. Stoeckenius, R. A. Bogomolni, Bacteriorhodopsin and related pigments of halobacteria. *Annu. Rev. Biochem.* **51**, 587–616 (1982).
51. R. R. Birge, Photophysics and molecular electronic applications of the rhodopsins. *Ann. Rev. Phys. Chem.* **41**, 683–733 (1990).
52. H. Ducklow *et al.*, "The marine system of the Western Antarctic Peninsula" in *Antarctic Ecosystems*, A. D. Rogers, N. M. Johnston, E. J. Murphy, A. Clarke, Eds. (Blackwell Publishing Ltd., 2012), 10.1002/9781444347241.ch5, pp. 121–159.
53. D. K. Steinberg *et al.*, Long-term (1993–2013) changes in macrozooplankton off the Western Antarctic Peninsula. *Deep Sea Res. Part I* **101**, 54–70 (2015).
54. T. R. Parsons, Y. Maita, C. M. Lalli, *A manual of chemical and biological methods for seawater analysis* (Pergamon Press, Oxford, 1984).
55. C. M. Moreno *et al.*, Molecular physiology of Antarctic diatom natural assemblages reveals multiple strategies contributing to their ecological success. bioRxiv [Preprint] (2023). https://doi.org/10.1101/2023.04.19.537459 (Accessed 20 April 2023).
56. C. M. Moreno, A. Marchetti, Metatranscriptomics of phytoplankton communities from the Western Antarctic Peninsula. Sequence Read Archive. https://www.ncbi.nlm.nih.gov/sra/?term=PRJNA877830. Accessed 8 September 2022.